Optical Layout of the TESLA 5 GeV Damping Ring

W. Decking
DESY, Notkestraße 85, 22603 Hamburg, Germany

February 2001

Abstract

The TESLA linear collider needs damping rings to achieve the required small transverse emittances for optimum luminosity. Due to the TESLA pulse structure the damping rings are about 17 km long. The resulting unusual ratio of circumference to energy leads to a large space charge tune shift. The originally proposed damping ring [1] has thus been redesigned for higher energy. This paper describes the optical design of the 5 GeV TESLA damping ring.

1 Introduction

The TESLA linear collider foresees the acceleration of low emittance electron and positron bunches. The transverse emittances as produced at the particle sources are several orders of magnitude larger than the required emittance for optimal linear collider operation. Damping rings are therefore necessary to reduce the transverse emittances. Damping is achieved through the process of radiation damping by synchrotron radiation in bending fields and energy gain in RF cavities. The design of the damping ring has to ensure a small emittance and a sufficient damping rate.

One main design criterion for the TESLA damping ring arises from the pulse structure of the linear collider. The acceleration of 2820 bunches in one pulse of ≈ 1 ms duration, respectively a bunch train length of approximately 300 km is foreseen. To keep the damping ring length reasonable, this bunch train has to be stored in a compressed mode with a much smaller bunch spacing as in the linear accelerator. Consequently, each bunch has to be injected and ejected separately. The ring length is then given by the bandwidth of the injection and extraction system. A bandwidth of 50 MHz (a bunch spacing of 20 ns) requires a ring length of 17 km. To avoid the cost for additional 17 km of ring tunnel, the most part of the damping ring will be installed in the linac tunnel [2]. Short return arcs requiring additional tunnels provide a small fraction of the circumference.

The final extracted transverse emittance (ε_f) is given by

$$\varepsilon_f = \varepsilon_{eq} + (\varepsilon_f - \varepsilon_{eq})e^{-2T/\tau_D} \tag{1}$$

where ε_i and ε_{eq} are the initial (injected) emittance and the equilibrium emittance respectively, τ_D is the damping time and T is the storage time (200 ms). The initial normalized positron emittance is 0.01 m, and ∼7 damping times (28 ms) are required to achieve the final design normalized emittance of 2×10^{-8} m. The injected electron beam — having been produced by a photoinjector as opposed to a target — has a much better beam quality ($\gamma\varepsilon_i \approx 10^{-5}$ m), and only requires 4 damping times.

The different injected beam sizes lead also to different requirements for the transverse and longitudinal acceptance. Asking for an acceptance proportional to $\approx 35\sigma$ leads to a normalized transverse acceptance of 0.012 m for the electron ring. With the same requirement the positron ring acceptance would have to be unacceptably large. The requirement for the acceptance of the positron damping ring is thus to accept the collimated phase space of the positrons after the pre-accelerator (≈ 0.04 m). The electron ring — being built equal to the positron ring — will then have the same acceptance. Potential relaxed tolerances or smaller apertures for the electron ring have not been exploited.

The target parameters for the TESLA damping ring are summarized in table 1. Figure 1 shows a sketch of the positron damping ring layout, with the long straight section, in-/ejection, wigglers, and RF placed in the main linac tunnel. Slight modifications of the arc geometry would allow to place the wiggler in the arc tunnel.

The ring circumference and the damping time are imposed by the linear collider requirements. Two free parameters can be chosen: the damping ring energy and the bending magnet field. Section 2 summarizes some scaling laws which allow to find the optimal parameters analytically.

The damping ring lattice can be divided in three separate parts: the arc, the wiggler section and the long straight sections in the linac tunnel. The optics of these sections will be described in section 3. Dynamic aperture and tolerances are summarized in sections 4 to 5.

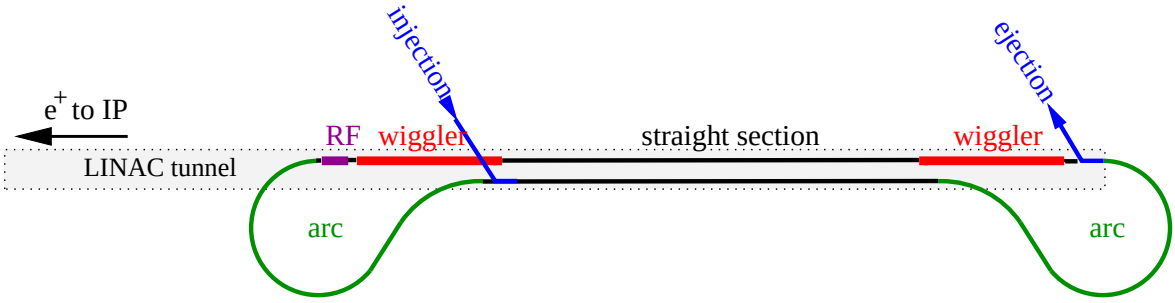

Figure 1: Conceptual layout of the positron damping ring. The electron ring is similar with the exception that the injection point is located close to the indicated ejection position at the beginning of the linac.

Table 1: Target parameters for the TESLA positron damping ring. Where different, values for the electron damping ring are given in parentheses.

Circumference C	17 km
Hor. extracted emittance $\gamma\varepsilon_x$	8×10^{-6} m
Ver. extracted emittance $\gamma\varepsilon_y$	0.02×10^{-6} m
Injected emittance $\gamma\varepsilon_{x(y)}$	0.01 m (10^{-5} m)
Number of damping times n_τ	7.2 (4.0)
Cycle time T_c	0.2 s
Damping time τ_d	28 ms (50 ms)
Number of bunches n_b	2820
Bunch spacing $\Delta\tau_b$	20×10^{-9} s
Number of particles per bunch N_e	2.0×10^{10}
Current	160 mA
Equilibrium bunch length σ_z	≈ 6 mm
Transverse acceptance $\gamma A_{x\|y}$	0.04 m (0.012 m)
Momentum acceptance A_p	1 % (0.5 %)

2 Damping Ring Scalings

The transverse damping time is:

$$\tau_D = \frac{2mc^2}{c}\frac{\gamma C}{J_{x(y)}U_0}$$

with the relativistic factor γ, ring circumference C, and damping partition numbers $J_{x(y)}$. U_0 is the energy loss per turn:

$$U_0 = \frac{2r_e mc^2}{3}\gamma^4 \int \frac{1}{\rho^2} ds \; .$$

In a wiggler based damping ring it is convenient to express the basic scaling laws in terms of the ratio of the wiggler to arc synchrotron radiation loss F_w:

$$F_w = \frac{L_{wig}/ < \rho^2_{wig} >}{2\pi F_D/\rho_{dip}} \tag{2}$$

with L_{wig} the total wiggler length, $< \rho^2_{wig} >$ the average square wiggler bending radius, ρ_{dip} the bending magnet radius and $2\pi F_D$ the total dipole bending angle of the ring [1]. With the above definition of F_w the damping time can be written as:

$$\tau_D = \frac{3}{r_e c} C \frac{1}{\gamma^3}\frac{\rho_{dip}}{2\pi F_D}\frac{1}{1+F_W} \tag{3}$$

[1] In usual circular accelerators $F_D = 1$, while the dog-bone damping ring requires $F_D \approx 2$, see figure 1.

yielding with the TESLA parameters ($F_D = 2$):

$$1 + F_w = 1.716 \times 10^{11}\,[\mathrm{m}^{-1}]\frac{\rho_{dip}}{\gamma^3}\,. \tag{4}$$

The horizontal equilibrium emittance can be calculated from:

$$\varepsilon_x \propto \frac{\gamma^2}{J_x}\langle\frac{H}{\rho}\rangle \tag{5}$$

with

$$H = \gamma D^2 + 2\alpha DD' + \beta D'^2 \tag{6}$$

with α, β, γ the Twiss parameters and D, D' the dispersion functions. $\langle\frac{H}{\rho}\rangle$ denotes the average around the ring.

The horizontal emittance is created both in the bending magnets and in the wiggler. The equilibrium emittance for bending magnets ε_{arc} and wigglers ε_{wig} can be calculated separately and combined to the total equilibrium emittance according to the following equation:

$$\varepsilon_x = \frac{1}{J_x + F_w}(\varepsilon_{arc}J_x + \varepsilon_{wig}F_w)\,. \tag{7}$$

Assuming a wiggler being placed in a dispersion free region its equilibrium emittance becomes [2]:

$$\gamma\varepsilon_{wig} \approx C_q 1.78 \times 10^6 B_{wig}^3 \lambda^2 < \beta > \tag{8}$$

with λ the wiggler period length, B_{wig} the maximum wiggler magnetic field, $< \beta >$ the average β-function in the wiggler and $C_q = 3.84 \times 10^{-13}\,\mathrm{m}$.

The emittance in the arc is

$$\gamma\varepsilon_{arc} = C_q\gamma^3 F_\varepsilon(lattice, \mu_x)\frac{1}{J_x}\theta_{dip}^3 \tag{9}$$

with θ_{dip} the dipole bending angle and F_ε the lattice quality factor. This factor will be discussed in section 3.1.

The remaining linear parameter which can be influenced by the lattice is the momentum compaction factor, which is created in the dispersive sections of the ring:

$$\alpha_c = \frac{1}{C}\int\frac{D}{\rho}ds\,.$$

The momentum compaction contribution of the arc cells can be calculated as:

$$\alpha_{c;arc} \approx \frac{2\pi F_D}{C}F_\alpha(lattice, \mu_x) \tag{10}$$

with $F_\alpha(lattice, \mu_x)$ a lattice dependent factor, which will also be discussed in section 3.1. The momentum compaction contribution of the wigglers is:

$$\alpha_{c;wig} \approx -\frac{1}{C}\frac{1}{96}\left(\frac{\lambda}{\rho_{wig}}\right)^2 L_{wig}\,. \tag{11}$$

[2]For the estimates of the wiggler contributions to the emittance and momentum compaction a wiggler with a rectangular field profile and a pole length of $\lambda/4$ has been assumed.

The damping ring design has to consider the incoherent space charge tune spread. This tune spread can get rather large due to the unusual ratio of ring length to energy. The space charge tune shift for a particle in the longitudinal bunch center is:

$$\Delta Q_{sc;x(y)} \approx \frac{C r_e N_e}{(2\pi)^{\frac{3}{2}} \gamma^2 \sqrt{\varepsilon_x \varepsilon_{x(y)}} \sigma_z} \tag{12}$$

with N_e the number of electrons/positrons per bunch and σ_z the bunch length. The bunch length is influenced by the damping ring momentum compaction factor and the RF parameters. The maximum bunch length is somewhat imposed by the bunch compressor system following after the damping ring and is 6 mm. With all other parameters in equation (12) fixed by the linear collider requirements the only free parameter is the energy.

A ring energy of 5 GeV has been chosen as a compromise between the need for higher energy to reduce space charge effects ($\Delta Q_{sc;y} \approx 0.23$) and damping wiggler costs, and a preferable lower energy which reduces the RF power needs and eases the design of the damping ring arcs. Combining equations (3) and (7) shows that at constant bending radius ρ_{dip} and damping time τ_D the emittance contribution of the arc scales with γ^6. A low emittance lattice in the arcs is thus increasingly important and will be described in section 3.1.

3 Damping Ring Optics

3.1 Choice of the Arc Lattice

Two different lattice types are investigated for the design of the arc lattice:

- A FODO cell with dipoles placed between focusing and defocusing quadrupoles.
- So-called minimum emittance type lattices (TME) with a dipole placed between focusing quadrupoles in such a way that the horizontal β- and dispersion-function has its minimum in the middle of the dipole. This lattice achieves the smallest possible emittance in a given dipole.

The optimum values for the minimum of the horizontal beta and dispersion function in the middle of the dipole of a TME cell scale with the dipole length:

$$\beta_{x,min} = \frac{1}{2\sqrt{15}} l_{dip} \qquad\qquad D_{x,min} = \frac{\theta_{dip} l_{dip}}{24} \tag{13}$$

The minimum lattice quality factor is

$$F_{\varepsilon;min}(TME) = \frac{1}{12\sqrt{15}} \tag{14}$$

at a phase advance of $\approx 280°$. A 'detuned' minimum emittance cell is characterized by the ratio of the reached emittance to the minimum possible emittance $\varepsilon_R = \varepsilon/\varepsilon_{min}$.

The β and dispersion functions scale roughly with this ratio and the phase advance is $\tan \mu_x = \sqrt{3}\varepsilon_R/(\sqrt{\varepsilon^2 - 1} - \sqrt{5})$ [3]. A numerical evaluation of the factor $F_\varepsilon(lattice, \mu_x)$ is displayed in figure 2 as a function of the phase advance per cell. The TME lattices have been matched for three different cases:

- Matching the β and dispersion function to the respective value of the 'detuned' minimum emittance cell (TME).
- Matching the phase advance per cell while keeping the cell length constant (TME2).
- Matching a cell with a combined function dipole at the position of the defocusing quadrupole (FOBO).

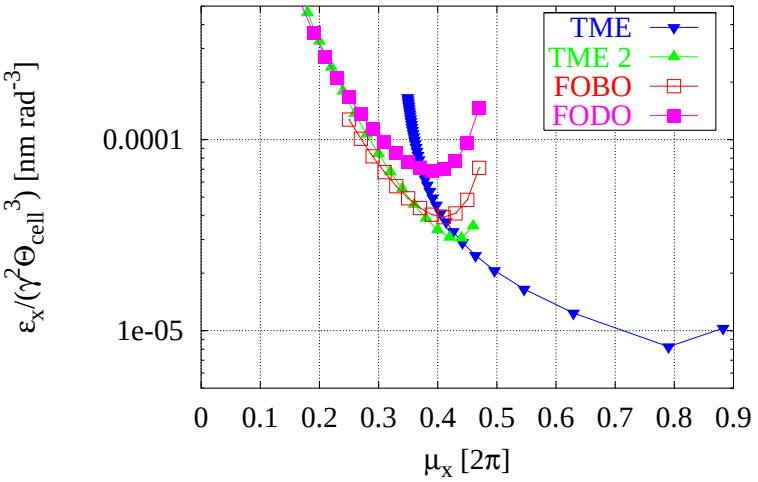

Figure 2: Comparison of emittance, normalized to $\gamma^2\theta_{cell}^3$ for TME, TME 2, FOBO and FODO cell.

The optimum horizontal phase advance for minimum emittance is usually not reached in real lattices. The strong focusing required leads to unacceptable dynamical behavior. A typical phase advance for a FODO cell is $\mu_{x;FODO} = 0.25$. The thus reached emittance is only 2 times larger than the smallest reachable one. For a TME lattice $\mu_{x;TME} \approx 0.4$ is a reasonable compromise, yielding a detuning of four. For these phase advances, a TME cell gives a ≈ 6 times smaller emittance for the same bending angle per cell, or a $\approx 6^{\frac{1}{3}}$ larger bending angle leads to the same emittance.

The simplest TME cell is the FOBO cell, made from a horizontally defocusing combined function dipole flanked by two focusing quadrupoles. The advantages of this cell is a small number of elements per cell, small space requirements, and a change of the damping partition number in the 'right' direction. The disadvantages are no flexibility and a poor separation of horizontal and vertical β-functions in view of the chromaticity correction. The advantage of shifting the damping partition numbers is negligible in the

dog-bone damping ring, as most of the damping is provided by the wigglers. Because of these reasons we will only consider a separate function dipole flanked by quadrupole doublets. This also gives flexibility in changing the phase advance if desired. The drift space between the two outer, focusing quadrupoles provides space for the focusing sextupole at highest horizontal dispersion and β-function (see figure 3).

Having selected the lattice type, the remaining parameter to be fixed is the length of the dipole magnet l_{dip}. The momentum compaction factor can be calculated using equation (10). The factor F_α is for the two lattice types [3]:

$$F_\alpha(FODO, \mu_x) \approx \frac{l_{cell}^2}{\rho_{dip}} \frac{1}{sin^2(\mu_x/2)} \tag{15}$$

$$F_\alpha(TME, \mu_x) \approx \frac{l_{dip}^2}{\rho_{dip}} \frac{\varepsilon_r + 1}{24} \tag{16}$$

The momentum compaction factor contribution of the wiggler is small due to the small dispersion in the wiggler. The momentum compaction factor is thus determined by the arc lattice. It is proportional to the dipole/cell length. We have thus chosen a rather long dipole magnet. This gives the disadvantage of increased arc- and thus tunnel-length. Additional benefits are larger optical functions, which lead to smaller sextupole strength and thus better dynamic properties of the lattice.

The dynamic aperture of a realistic ring made out of FODO cells or TME cells has been compared with the help of tracking calculations. A TME cell with a bending angle of $\theta_{dip} = 12^\circ$ has been designed. This compares with the bending angle of $\theta_{cell} = 7.5^\circ$

[3]For the FODO cell a placement of the dipoles in the middle between the quadrupoles has been assumed.

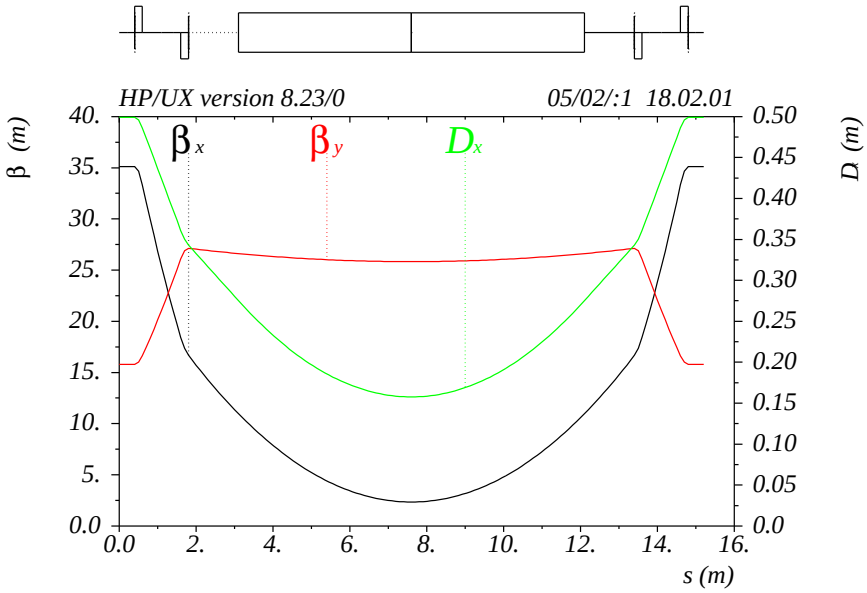

Figure 3: ARC bending magnet cell.

Table 2: Arc parameters.

Cell length	15.2 m
Cell phase advance $\mu_x/2\pi$, $\mu_y/2\pi$	0.4 ,0.1
Total number of cells	100
Length of one arc	950 m
Total chromaticity contribution ξ_x, ξ_y	-90 , -35
Total energy loss contribution	1.1 MeV/turn
Arc equilibrium emittance $\gamma\varepsilon_{arc}$	3.7×10^{-5} m
Total emittance contribution $\gamma\varepsilon_{arc}/(1+F_w)$	2.0×10^{-6} m

for the FODO cell used in the damping ring proposed in [1]. The dipole length has been set to 9 m to reach a comparable momentum compaction. The phase advance has been chosen to $\mu_x = 0.4$, $\mu_y = 0.1$. The resulting ring shows a two times larger dynamic aperture. Thus a TME lattice has been chosen for the damping ring arcs.

To achieve the desired emittance at an energy of 5 GeV the bending angle has been halved without changing the dipole length. A comparable FODO lattice would have $6\frac{1}{3}$ more cells and the dipole is ≈ 2.5 times shorter for the same momentum compaction. Figure 3 shows the TME arc cell with a 6 ° bending magnet.

The optical parameters of the damping ring arc are summarized in table 2. The geometry of the arc is optimized as a compromise between the tunnel length and the smallest number of cells. The influence of the 'reverse' bend angle α on the arc tunnel length is shown in figure 4. The total number of bending cells is 50, corresponding to a 'reverse' bend angle of 60 ° . The layout of one arc is shown in figure 5.

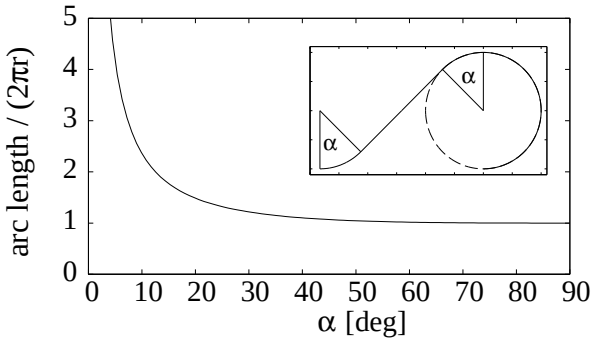

Figure 4: Dependence of total arc tunnel length on 'reverse' bend angle α.

The transformation between the positive and negative bending arc section is done via a zero dispersion FODO lattice. The length is adjusted to provide ≈ 0.5 m space between the two beam lines in the linac tunnel. The dispersion suppression consists of a half dipole scheme. The same suppressor is used at the end of the arc. Figure 6 displays the dispersion suppressor and two FODO cells.

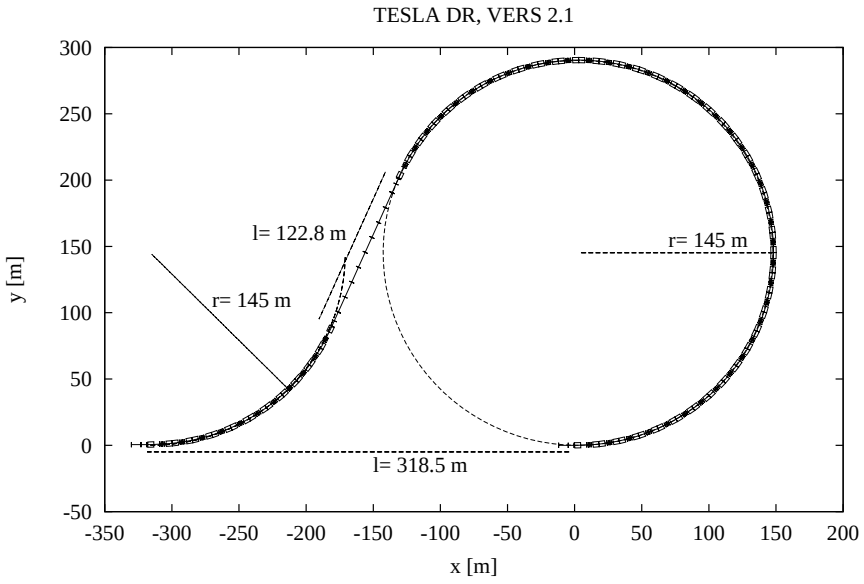

Figure 5: Layout of one damping ring arc.

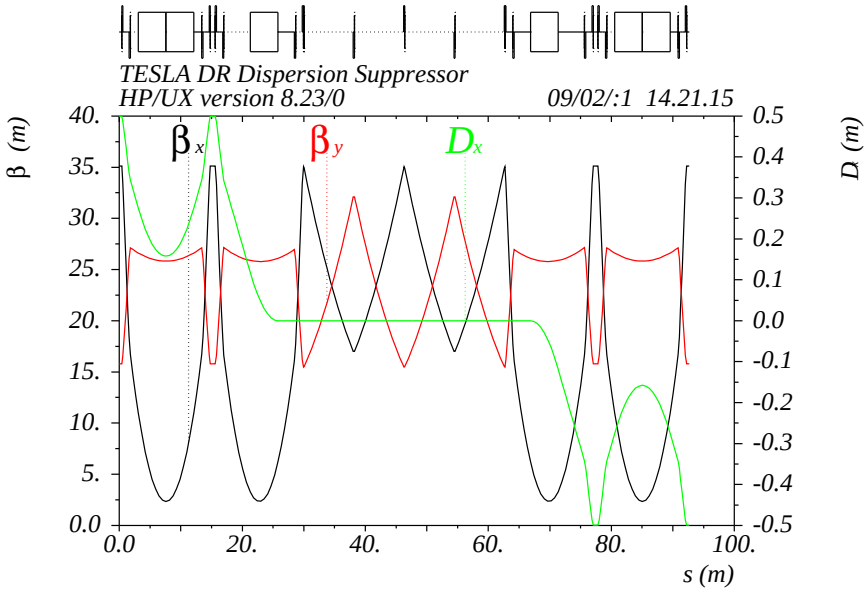

Figure 6: Transformation between positive and negative bending cell.

3.2 Wiggler Cell

Two alternative designs for the damping wigglers have been studied: permanent magnet [4] and electromagnetic [5] technology. The permanent magnet wigglers advantages are compact size and low operating costs. On the other hand, an electromagnetic wiggler is tunable and less sensitive to radiation damage. Due to cost and space constraints, the maximum current density in the electromagnetic wiggler is limited and the power requirements for the electromagnetic wiggler system would be 6.8 MW. Therefore the

permanent magnet wiggler has been chosen as the reference design for the damping ring. Radiation damage can be avoided by means of collimation and an active protection system.

In respect of the optical design of the wiggler cell the choice of the wiggler technology is not important. The electromagnetic wiggler will produce a larger horizontal emittance due to its longer period length and higher field.

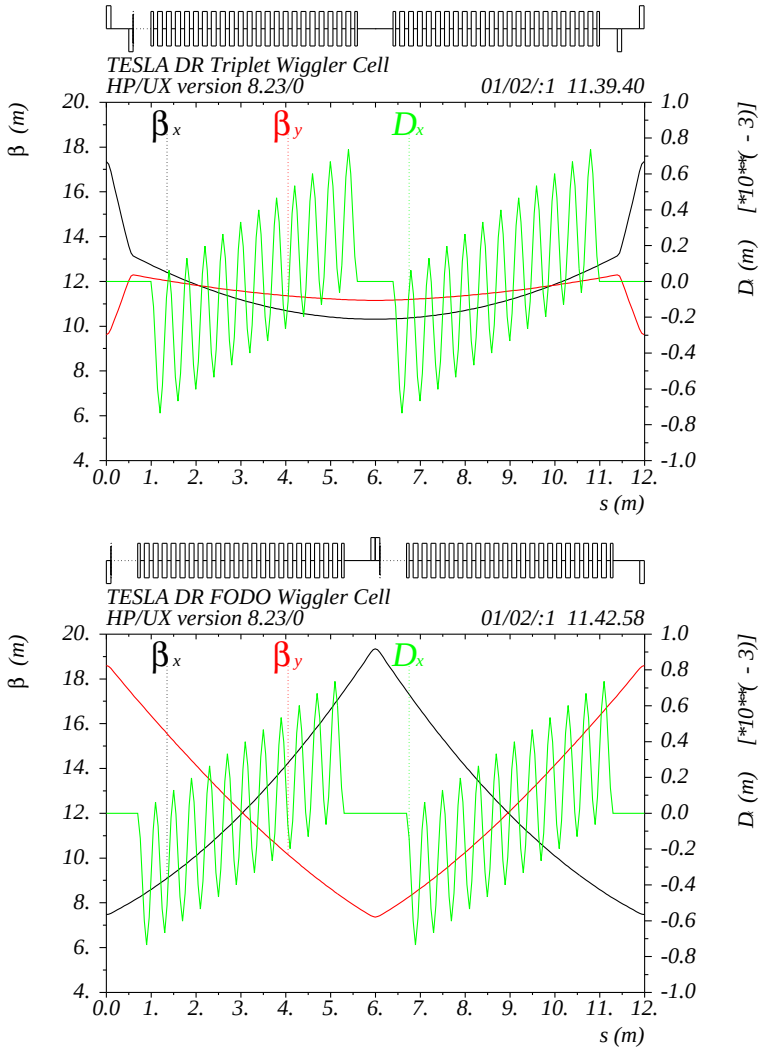

Figure 7: Wiggler cell using a triplet focusing lattice (upper) or a FODO lattice (lower).

The $\approx 5\,\mathrm{m}$ long wigglers can be embedded in a FODO or triplet focusing structure (see figure 7). The horizontal phase advance can be varied to obtain the desired horizontal emittance. The vertical phase advance is chosen as a compromise between a small contribution to the total chromaticity of the ring and the required vertical aperture at injection. Assuming an inner half aperture of 10 mm and an additional safety margin of 2 mm for orbit missteering and misalignment the largest β-function for the injected positron beam is $\beta_{max;y} = (8 \times 10^{-3})^2 / \frac{0.036}{\gamma} = 17.4\,\mathrm{m}$.

The maximum β-function in a FODO lattice is determined by the phase advance and the cell length and is $\approx 1.75 - 2 \times l_{cell}$ for phase advances between 45° and 115°. This limits the FODO cell length to 10 m. The wiggler design gets easier and more efficient with increasing wiggler length (less end poles, connections, etc.) and thus a longer cell may be desirable. The triplet focusing allows to confine the vertical β-functions while simultaneously tuning the average horizontal β for emittance control. The disadvantages of the triplet lattice are the need of one more quadrupole per cell. Both lattice types can easily be accommodated in the damping ring. The final choice of the lattice should be done together with the final optimization of the wiggler parameters.

The equilibrium emittance due to the wiggler cell has been calculated for both lattices and various horizontal phase advances. The vertical phase advance has been kept at 45°. Figure 8 gives the horizontal emittance and the chromaticity of one wiggler cell. The total chromaticity contribution of the wiggler section is $\approx 10\,\%$ of the total ring chromaticity. Table 3 summarizes the wiggler section properties.

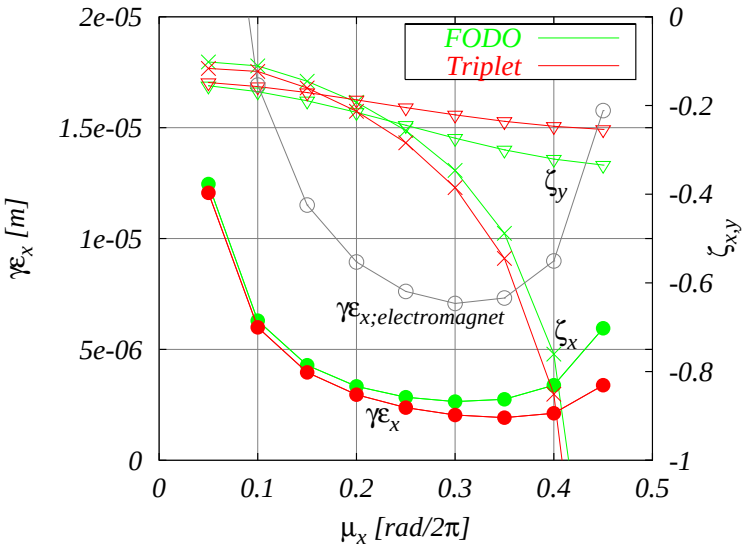

Figure 8: Normalized horizontal equilibrium emittance and chromaticities for permanent magnet wiggler embedded in a FODO or triplet lattice.

3.3 Other Sections of the Ring

3.3.1 Long Straight

The long straight section consists of 100 m long FODO cells. Their number has been adjusted to provide a 17 km long ring. The phase advance is $\mu_{x,y} = 0.125$, which yields a maximum beta-function of ≈ 200 m. The contribution to the total chromaticity is about 15 % horizontally and 25 % vertically.

Table 3: Wiggler section parameters for both electromagnet and permanent magnet designs.

Cell length	12.2 m	
Cell phase advance $\mu_x/2\pi$, $\mu_y/2\pi$	0.075 ... 0.3, 0.125	
Cell chromaticity ξ_x, ξ_y	–0.05 ... –0.32, –0.14 ... –0.28	
Maximum vertical beta	18 ... 28 m	
Energy loss contribution	19.1 MeV/turn	
Radiated power (160 mA)	3 MW	
	Permanent magnet	Electro-magnet
Total number of cells	45	36
Wiggler equilibrium emittance $\gamma\varepsilon_{wig}$	$(7.4 \ldots 2.4)\times10^{-6}$ m	$(19.6 \ldots 6.1)\times10^{-6}$ m
Emittance contribution $\gamma\varepsilon_{wig}\frac{F_w}{1+F_w}$	$(7.8 \ldots 2.5)\times10^{-6}$ m	$(20.7 \ldots 6.5)\times10^{-6}$ m
gap g	25 mm	25 mm
period length λ	0.40 m	0.55 m
number of periods	12	8
peak field B_{max}	1.68 T	1.8 T
field integral $\int B^2 ds$	1.37 Tm/m	2.1 Tm/m
magnet length for $\int B^2 ds = 605\,\mathrm{T^2m}$	468	300

The TESLA tunnel follows the curvature of the earth, and thus the straight sections require vertical bending. The emittance contribution of the vertical bending magnets is negligible, but care has to be taken to have no vertical dispersion in the wiggler and arc sections.

Table 4: Parameters for the damping ring straight sections.

Cell length	100 m
Cell phase advance $\mu_x/2\pi$, $\mu_y/2\pi$	0.125, 0.125
Total number of cells	140
Chromaticity contribution ξ_x, ξ_y	-18, -18

3.3.2 Coupling Insertion

A further decrease of the incoherent space charge tune shift is possible with a local increase of the beam size. For this purpose coupling insertions at the beginning and end of the long straight section are used. By means of a skew quadrupole triplet the initial distribution is transformed in a vortex distribution with the particle trajectories rotating in the x-y plane [6]. The resulting vertical and horizontal beam sizes are equal and $\sqrt{2}$ time smaller than the initial horizontal beam size. The rotation is removed from the beam with a similar triplet with the only requirement that the phase advances

between the two insertions have to be equal. Figure 9 shows the projected horizontal and vertical beam sizes in a short beamline sequence for no coupling insertion (left) and coupling insertion included (right). With this coupling insertion the space charge tune shift can be reduced by approximately a factor of 5. This is sufficient for operation of the damping ring at small vertical emittances [7].

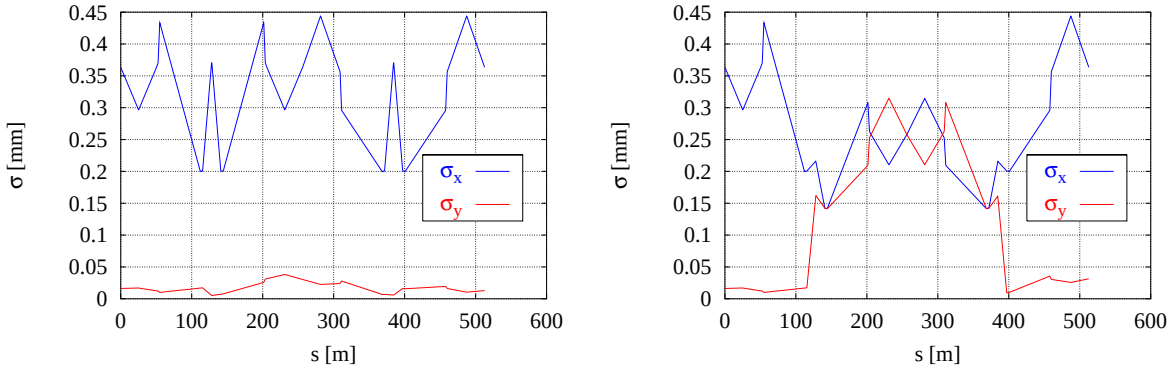

Figure 9: Projected horizontal and vertical beam size along a beam line sequence with no coupling insertion (left) and coupling insertion included (right).

3.3.3 Injection and Extraction

In- and ejection will take place in the straight sections of the damping ring. The inner radius of the foreseen injection kickers is 25 mm, leading to a maximum β-function of 50 m to allow sufficient aperture at injection. The kick strength for both injection and ejection is $\theta \approx 0.6\,\text{mrad}$ or $\int Bdl \approx 0.01\,\text{Tm}$ at 5 GeV and $\beta_{kicker} = 50\,\text{m}$. To ensure an ejected beam stability of $< 0.1\sigma_x$, the amplitude stability of the kicker system has to be $7 \times 10^{-6}\,\text{Tm}$ for both the maximum deflection and the remaining ripple after the kicker pulse; this corresponds to a relative stability of 7×10^{-4} at maximum deflection. Reduction of the relative stability requirement cannot be achieved using (for example) an orbit bump at the ejection septum, since the full aperture of the machine is required for the undamped bunches[4].

Depending on the kicker/pulser combination to be installed, 10 to 20 kickers of $\approx$ 0.5 m [8] length will be installed. The ejection section will host all of them in one common straight section, followed by the septum after a phase advance of 90°. The ejection section is located at the beginning of the linac in the main linac tunnel. Therefore it has been designed as short as possible (see figure 10).

[4]Damped and undamped bunches are simultaneously present in the ring.

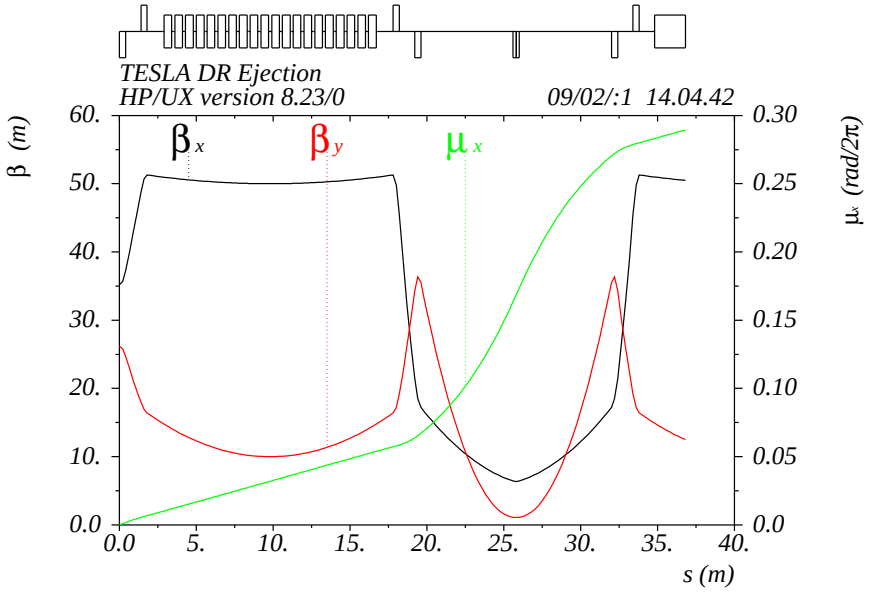

Figure 10: Injection lattice with 20 kickers in the straight section on the left side and the septum on the right.

4 Dynamic Aperture

The dynamic properties of the damping ring are completely determined by the strong sextupoles. These sextupoles are placed in the arcs and have to provide the chromaticity correction for the whole ring.

The dynamic aperture has been optimized in the following way:

- The position of the sextupoles in the arc cell has been chosen such that their strength is minimal.
- The phase advance per cell has been chosen to achieve cancelation of driving terms after a certain number of cells. This cancelation is perfect only for on-energy particles.
- The second order dispersion has been canceled at the end of the arcs.

The dynamic aperture has been calculated with particle tracking. The tracking included misalignment errors to simulate a coupling ratio of $\varepsilon_y/\varepsilon_x = 1\,\%$ and a β-beat. The real physical aperture has been included in the tracking [5]. Results of the tracking are shown in figure 11.

[5]The physical aperture of the damping ring is ≈ 1.7 times the injected beam size with the exception of the wiggler section where the vertical aperture is reduced to ≈ 1.4 times the injected beam size. If required this aperture can be enlarged by changing the vertical β-function (see section 3.2).

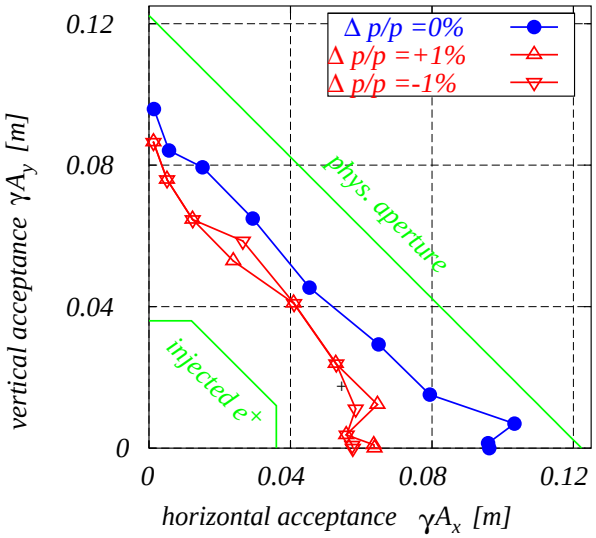

Figure 11: Dynamic acceptance of the damping ring. The simulations include quadrupole and sextupole alignment errors which result in an average emittance coupling of 1 %, and the real physical aperture as the maximum amplitude limit. The phase space volume of the incoming beam as defined by acceptance of the positron pre-accelerator is also shown.

5 Tolerances

Figure 12 shows a comparison of the unnormalized horizontal and vertical emittance of various low emittance synchrotron radiation sources and planned or existing damping rings. The required emittance of the TESLA damping ring for a damping ring energy range from 2 GeV to 5 GeV is given.

The required horizontal emittance of the TESLA damping ring is only a factor of two smaller than the emittance obtained at the ATF [11]. The final vertical emittance is a factor of 4 smaller than the smallest vertical emittance achieved at the ESRF [12]. Emittance ratios of $\approx 0.2\,\%$ have been obtained in various synchrotron radiation sources and collider rings [12, 13, 14]. Achieving the design emittance for the damping ring should thus not be a principal problem. Tight alignment tolerances and high resolution orbit diagnostics are crucial.

Vertical emittance is generated through betatron coupling and residual vertical dispersion. Betatron coupling can be reduced with the help of skew-quadrupoles. Minimizing spurious vertical dispersion in the wigglers is especially important: here the vertical rms dispersion has to be corrected to the 1 mm level. An algorithm which performs a simultaneous orbit and dispersion correction has been studied. The simulations included alignment errors assigned to all machine elements (as summarized in table 5). Successive steps of the correction algorithm were applied until no further reduction of the residual rms orbit and dispersion were achieved. Studies using many random error seeds showed that the required vertical emittance was obtained on average. Correcting the dispersion to the required 1 mm in the wiggler sections requires a

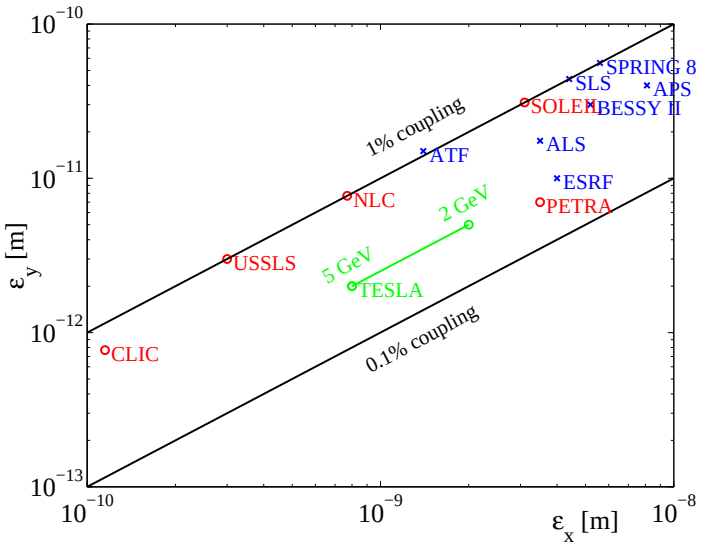

Figure 12: Unnormalized horizontal and vertical emittance of some present day (blue crosses) and planned (red circles) synchrotron radiation sources and damping rings. For existing rings the best quoted coupling ratio is given. The values for CLIC and NLC have been taken from [9, 10]. The rings operate at an energy between 1 GeV and 8 GeV.

Table 5: Alignment tolerances for the damping ring.

Transverse position of elements	0.1 mm
Roll angle	0.2 mrad
BPM resolution	0.01 mm
BPM resolution wiggler section (averaging mode)	0.001 mm

relative orbit measurement with a precision of $\sim 1\mu$m. Beam position monitors (BPM) with a resolution of 10 μm will be used in the damping ring. For the high-precision dispersion measurement the accuracy can be achieved by averaging.

The dispersion can also be corrected using empirical tuning of the vertical beam size (emittance) with the appropriate dispersion generating orbit bumps; this method has the advantage of not requiring an explicit measurement of the dispersion function.

An important concern is the orbit stability over various time scales. For long-term stability a diffusion-like orbit drift caused by slow uncorrelated ground motion must be taken into account. An orbit correction back to the 'golden' orbit is necessary every few minutes to avoid unacceptable vertical emittance blow-up. For this task a BPM resolution of 10 μm is sufficient once the vertical emittance has been optimized (i.e. the 'golden' orbit established). On the short time scale the influence of time varying stray fields in the long straight sections is a concern. With no active correction applied to the orbit, the stray field amplitude has to be smaller than a μT. This is in contradiction to measurements on the DESY site, where field amplitudes up to several μT have been

observed in typical accelerator environments. Thus a fast orbit feedback has to control the resulting residual orbit in the wiggler and arc sections of the ring, or the vacuum chamber must be magnetically shielded.

6 Summary

The optical layout of the 5 GeV TESLA damping ring consists of an arc lattice based on long minimum emittance cells, an approximately 500 m long wiggler insertion and approximately 14 km long straight sections. Special optical insertions provide full betatron coupling in the straight sections. The dynamic aperture of the proposed design is sufficient to accommodate the injected positron beam. The desired vertical emittance cam be achieved with an high accuracy dispersion measurement and correction. Table 6 summarizes the main damping ring parameters.

Table 6: Parameters for the TESLA positron damping ring. Where different, values for the electron damping ring are given in parentheses.

Energy E	5 GeV
Circumference C	17 km
Hor. extracted emittance $\gamma\varepsilon_x$	8×10^{-6} m
Ver. extracted emittance $\gamma\varepsilon_y$	0.02×10^{-6} m
Injected emittance $\gamma\varepsilon_{x(y)}$	0.01 m (10^{-5} m)
Number of damping times n_τ	7.2 (4.0)
Cycle time T_c	0.2 s
Damping time τ_d	28 ms (50 ms)
Number of bunches n_b	2820
Bunch spacing $\Delta\tau_b$	20×10^{-9} s
Number of particles per bunch N_e	2.0×10^{10}
Current	160 mA
Energy loss/turn	21 MeV (12 MeV)
Total radiated power	3.2 MW (1.8 MW)
Tunes Q_x, Q_y	72.28 , 44.18
Chromaticities ξ_x, ξ_y	-125 , -68
Momentum compaction α_c	0.12×10^{-3}
Equilibrium bunch length σ_z	6 mm
Equilibrium momentum spread σ_p/P_0	0.13 % (0.1 %)
Transverse acceptance $\gamma A_{x\|y}$	0.05 m
Momentum acceptance A_p	1 %

References

[1] R. Brinkmann, G. Materlik, J. Roßbach, A. Wagner (editors), *Conceptual Design of a 500 GeV e+e- Linear Collider with Integrated X-ray Laser Facility*, DESY 97-048 and ECFA 97-182, 1997, chapter 3.

[2] K. Flöttmann, J. Rossbach, *Emittance Damping Considerations for TESLA*, DESY 93-023, 1993.

[3] J.P. Potier, L. Rivkin, *A low Emittance Lattice for the CLIC Damping Ring*, Proc. Part. Acc. Conf., Washington 1997, p. 476.

[4] M. Tischer, J. Pflüger, W. Decking, *A Permanent Magnet Damping Wiggler*, TESLA 2000-40, 2000.

[5] S. Guiducci et. al., *Technical Layout of the TESLA Damping Ring*, LNF-01/003 (NT), 2001.

[6] Y. Derbenev, *Adapting Optics for High Energy Electron Cooling*, University of Michigan Preprint, 1998.

[7] W. Decking, R. Brinkmann, *Space Charge Problems in the TESLA Damping Ring*, Proc. Europ. Part. Acc. Conf., Wien 2000, p. 1024.

[8] B.I. Grishanov, F.V. Podgorny, J. Ruemmler, V.D. Shiltsev, *Very Fast Kicker for Accelerator Applications*, TESLA 96-11, 1996.

[9] J. Jowett, H. Owen, *Damping Rings for CLIC at 3 TeV*, Transparencies CERN AP Forum, wwwslap.cern.ch/ frankz/CLIC/www2/APFORUM.pdf, 2000.

[10] P. Emma, *Preliminary Main Damping Ring Design for the NLC (Version 2.0)*, http://www-project.slac.stanford.edu/lc/local/notes/dr/NLCMDR1.pdf, 1999.

[11] J. Urakawa, *Experimental Results and Technical Research and Development at ATF (KEK)* Proc. Europ. Part. Acc. Conf., Wien 2000, p. 63.

[12] R. Nagaoka, *Work Carried Out at the ESRF to Characterize and Correct the Coupling*, Proc. Europ. Part. Acc. Conf., Wien 2000, p. 131.

[13] E.B. Blum, *Operation of a Low Emittance Lattice at the NSLS X-RAY Ring*, Proc. Part. Acc. Conf., New York 1999, p. 2304.

[14] M. Zobov, *Status Report on DAΦNE Performance*, Proc. Europ. Part. Acc. Conf., Wien 2000, p. 43.

[15] H. Grote, F. Iselin, *The MAD Program*, CERN/SL/90-13(AP), 1996.